IEEE Access
Multidisciplinary | Rapid Review | Open Access Journal

Received February 7, 2021, accepted February 22, 2021, date of publication March 4, 2021, date of current version March 15, 2021.

Digital Object Identifier 10.1109/ACCESS.2021.3064016

Current and Speed Sensor Fault Diagnosis Method Applied to Induction Motor Drive

CUONG DINH TRAN[1], PETR PALACKY[2], MARTIN KUCHAR[2], PAVEL BRANDSTETTER[2], AND BACH HOANG DINH[1]

[1]Power System Optimization Research Group, Faculty of Electrical and Electronics Engineering, Ton Duc Thang University, Ho Chi Minh City 700000, Vietnam
[2]Faculty of Electrical Engineering and Computer Science, VSB-Technical University of Ostrava, 708 00 Ostrava, Czech Republic

Corresponding author: Martin Kuchar (martin.kuchar@vsb.cz)

This work was supported by the Research of Modern Control Methods of AC Controlled Drives, VSB-Technical University of Ostrava, 2021, under Project SP2021/70.

ABSTRACT The paper proposes a novel approach based on a current space vector derived from measured stator currents to diagnose speed and current sensor failures in the field-oriented control of induction motor drives. A comparison algorithm between the reference and measured rotor speed is used to detect the speed sensor faults. A counter is added to eliminate the influence of the encoder noise in the diagnosis method. In this approach, estimated quantities are not used in the proposed speed sensor fault diagnosis strategy, which increases the independence between the diagnosis stages in the fault-tolerant control (FTC) method. Moreover, in order to discriminate between the speed sensor faults and the current sensor faults, a new approach combining the current space vector and a delay function is proposed to reliably determine the current sensor failures. The MATLAB-Simulink software was used to verify the idea of the proposed method. Practical experiments with an induction motor drive controlled by DSP TMS320F28335 were performed to demonstrate the feasibility of this method in practice. The simulation and experimental results prove the effectiveness of the proposed diagnosis method for induction motor drives.

INDEX TERMS Fault-tolerant control, diagnosis, induction motor, FOC, sensorless control.

NOMENCLATURE

$\boldsymbol{\Psi}_S^S$	*Stator flux vector in* $[\alpha, \beta]$ *coordinate system*
$\boldsymbol{\Psi}_R^S$	*Rotor flux vector in* $[\alpha, \beta]$ *coordinate system*
$\boldsymbol{i}_S^S$	*Stator current vector in* $[\alpha, \beta]$ *coordinate system*
$\boldsymbol{i}_R^S$	*Rotor current vector in* $[\alpha, \beta]$ *coordinate system*
$\boldsymbol{u}_S^S$	*Stator voltage vector in* $[\alpha, \beta]$ *coordinate system*
$u_{S\alpha}, u_{S\beta}$	*Stator voltage components in* $[\alpha, \beta]$ *system*
u_{Sx}, u_{Sy}	*Stator voltage components in* $[x, y]$ *system*
u_a, u_b, u_c	*Stator voltage components in* $[a, b, c]$ *system*
i_{Sx}	*Flux current component*
i_{Sy}	*Torque current component*
i_m	*Magnetizing current*
R_S, R_R	*Stator and rotor resistance*
L_S, L_R	*Stator and rotor inductance*
L_m	*Magnetizing inductance*
T_R	*Rotor time constant*
T_S	*Stator time constant*
ω_m	*Mechanical angular speed*
ω_{en}	*Measured rotor speed from the encoder*
p	*Pole pair number*
γ	*Rotor flux angle*

The associate editor coordinating the review of this manuscript and approving it for publication was Wenbing Zhao.

I. INTRODUCTION

In recent years, induction motor drive (IMD) systems overcame the challenges of complex nonlinear control structures to become the most common machine type for applications in industry and electric cars, HVAC, home appliances, etc. Generally, a typical IMD system consists of four essential parts: an induction motor (IM), a power converter, measurement sensors, and a controller [1]. To control the induction motor operating at a specific speed, the controller uses feedback measurement signals from sensors and compares them to desired values to generate a control command for a power converter supplying an IM. This process performance relates to the control algorithm ability and the quality of

hardware devices in which the sensor system keeps a significant position. Recently, sensor fault diagnosis is an exciting and necessary topic in controlling IMDs. In industrial safety crucial applications such as electric vehicles, ventilation systems, conveyor systems, etc., it is essential to integrate a fault-tolerant control (FTC) function into the control process against the sensor faults [2], [3]. The FTC techniques consist of two main groups: passive FTC (PFTC) and active FTC (AFTC) [4]. In PFTC, the control system of IMDs can only deal with simple sensor failures and work offline. However, AFTC is more effective because it can deal with more difficult sensor failures and work online. AFTC includes three main steps: fault diagnosis, isolation, and reconfiguration [4]. In the measurement system of IMDs, there are three primary sensor types commonly used to provide feedback signals, i.e., speed encoders, current sensors, and dc-link voltage sensors. However, the voltage sensors are less important than the speed or current sensors in modern control schemes where the control loop reference voltage can replace the voltage signal. Therefore, this research aims to propose an improving AFTC method against the speed sensor and current sensor faults.

Most speed sensor diagnosis methods are based on supervising the difference between a measured rotor speed signal and an estimated speed value for detecting speed sensor faults. If the deviation exceeds a specific threshold, it can be determined the failure state of the speed sensor. In [5], a comparison algorithm between the measured rotor speed and an estimated speed signal of the extended Kalman filter (EKF) was applied to detect the speed sensor failure. Moreover, the authors have proposed two techniques called hybrid-FTC and generalized internal mode-control for the reconfiguration phases. Simulation results confirmed the effectiveness of this method in the sensor fault diagnosis. Another approach uses an adaptive stator flux observer to estimate the rotor speed, as presented in [6]. The diagnosis algorithm has based on the error between the estimated speed value and the speed sensor signal to decide whether a faulty state occurred or not. That error has also be refined by a low-pass filter before compared to a predefined threshold. In [7], a maximum-likelihood-voting diagnosis algorithm is applied to detect speed sensor failures. In this algorithm, probability coefficients of a feedback speed signal and two estimated speed signals from the EKF and Luenberger Observer are used to diagnose when the speed fault occurrence and optimize the IM performance in the entire speed-range. Simulation and experimental results have demonstrated the effectiveness of this method. In [8], a proposed algorithm uses the stator currents to diagnose the speed sensor failures [8]. The advantage of this method is the ability to separate the diagnosis and reconfiguration stages. In this case, estimated currents are used for the fault detection, and speed sensorless control (model reference adaptive system - MRAS) is used in the reconfiguration phase.

Furthermore, the field-oriented control (FOC) scheme was first proposed by Hasse (1969) and Blaschke (1972). It has been considered as a typical modern control technology of IMDs. In this method, the role of the stator currents is essential for the control of IMD systems. The advantage of the FOC method is precise control of both the flux and the torque of IMs [9]–[11]. The main idea of the FOC is to separate the stator current vector into two components, the x-component corresponding to the rotor flux axis and the y-component perpendicular to the x-axis. The x-component of the stator current vector varies the rotor flux, and the y-component of the stator current vector is used to control the torque. Thus, the stator currents feedback signals play an essential role in the control loops-based FOC, and the sudden lack of the feedback current signals can cause the IMD controllers to fail and it can finally lead to IMD damage. As a result, FTC against the current sensor fault is essential for IMDs using the FOC technique.

Typically, three-phase induction motors use three current sensors to measure the stator phase currents. According to Kirchhoff's current law, if one current sensor fault occurs, the diagnosis algorithm can detect that error by comparing the three current values and their corresponding estimated current values [12], [13]. It means that the current status of one specific phase, e.g., phase-A current, can be supervised by two measured currents of remaining phases, i.e., phase B and C currents. The fault detection algorithm is based on comparing three measured current space vectors (CSV) and one estimated current space vector to determine the faulty phase exactly. The three measured signals based CSVs, each of which consists of two measured current values and one remaining value estimated from Kirchhoff's current law, are compared to the estimated CSV to generate the comparison indexes. Hence, the faulty current sensor in a specific phase can be identified by the smallest comparison index corresponding to a specific measured CSV. However, the idea of using Kirchhoff's current law mentioned above is unable to apply for IMDs installed with two current sensors only. Thus another approach using the peak values of measured and estimated currents at one electrical cycle [14] has been proposed to produce two comparison indexes, each of which is correspondent to one specific current phase. Both indexes are zero at normal operation, but if there is one current sensor broken, the corresponding index will significantly increase. As a result, the specific phase of a faulty sensor can be precisely detected by supervising the comparison indexes. As another methodology, the axes transformation method [15] has been proposed to determine a fault in phase current sensors. In this idea, firstly, the measured current signals of two phases are transformed into two different $[\alpha, \beta]$ coordinate systems corresponding to each phase stator current. Then, the reference stator currents in $[x, y]$ rotating coordinate system and rotor flux angle have been used to calculate two estimated stator current units corresponding to those such two phases in $[\alpha, \beta]$ coordinate. Finally, each pair of the measured and estimated signals has connected to one observer corresponding to a specific phase stator current; thus, we have two separate observers in the detection algorithm. When occurring a failure in any phase current sensor, the significant errors are obtained at both α and β axes of the observer

representing that faulty phase, but in the remaining observer, it only arises at β axes. As a result, the position of the faulty current sensor can be determined precisely. Another strategy in [16] has applied an improving diagnosis method based on specific features of the FOC to determine the position of a faulty current sensor where the root means square (RMS) values of two-phase currents are calculated and subtracted from each other to generate a checking index. If this index is greater than a specific threshold, that means there is a current sensor fault occurrence. The authors use an ''isolation gain parameter'' created from the current components along the y-axis, combining with the measured A-phase current, to locate a faulty current sensor. This method is simple and independent of the machine model.

In fact, most common FTC methods include two main steps: the fault diagnosis and the reconfiguration steps. This research proposes a novel fault diagnosis methodology based on the feedback signals from sensors and current space vectors to detect the faulty conditions for both the speed sensor and the current sensors. If a sensor failure state is detected, a sensorless control scheme is applied to reconfigure the controllers diagram of an IMD. Thus, the proposed FTC is developed to deal with both speed and current sensor failures. However, the proposed FTC can deal with a single faulty sensor only, either speed or current sensor failures, not both speed and current sensor damaged at the same time. The probability of two sensor types (speed and current) damaged simultaneously is very low in practice. Therefore, the proposed approach can stably work if the speed sensor is damaged, but two current sensors are still healthy. Similarly, even when two current sensors are broken, it also works stably if the speed sensor is good. Moreover, the proposed diagnosis method can exactly discriminate between the speed sensor fault and the current sensor fault as well as the position of faulty sensor phases.

The proposed diagnosis methodology ideas have been derived from experimental experiences and the features of the FOC scheme of IMDs; thus, it effectively operates in practice. The main contributions of this research are the following:

- The paper proposes a new approach to detect the speed sensor fault by comparing the reference rotor speed and the feedback sensor speed. That faulty sensor status is confirmed only if the failure duration exceeds a preset threshold in a time counter. The execution time of speed sensor fault detection is 3 ms and it can be applied for various speed sensor faults including infinite, zero, or any other incorrect values.
- The paper proposes a new approach called the delay algorithm to detect phase-current sensor faults. It is based on the comparison between a present instantaneous value of the sinusoidal current signal and a stored value of the same signal from the previous sampling cycle. This approach is simple, reliable, and effective; thus, it is convenient for practical applications.
- The paper presents an effective FTC approach that deals with the failures of the speed and current sensors. It works well with the damaged speed sensor and two healthy current sensors or even two broken current sensors (all current sensors of the drive) and the healthy speed sensor.
- According to [17], the sensorless control schemes based IMDs often have some operational difficulties in low-speed operation because of the machine parameters sensitivity, inverter nonlinearities as well as increasing the processing time of the control algorithm. However, the proposed FTC approach effectively deals with abnormal operations of the IMD in a low-speed zone.

Simulations in Matlab Simulink, as well as practical experiments, have been implemented to demonstrate the effectiveness of the proposed technique. The simulation and experimental results have proved the proposed method ability in various test cases, especially in low-speed ranges.

The paper structure consists of five sections. This part introduces the considered problem, the second part contains a mathematical description of the IMD and the proposed algorithm. The two following sections present the simulation and experimental results, respectively to demonstrate the effectiveness of the method. The last section summarizes the contributions and future expectations of this research.

II. CURRENT AND SPEED SENSOR FAULT-DIAGNOSIS ALGORITHM

A. MATHEMATICAL MODEL OF INDUCTION MOTOR AND SENSOR FAULT TYPES

As applying modern control methods, IMDs can precisely control both the flux and torque simultaneously. Generally, the control methods are based on the dynamic model of induction motors, which is described in the $[\alpha, \beta]$ coordinate system as follows:

$$\boldsymbol{u}_S^S = R_S \boldsymbol{i}_S^S + \frac{d\boldsymbol{\Psi}_S^S}{dt} \tag{1}$$

$$0 = R_R \boldsymbol{i}_R^S + \frac{d\boldsymbol{\Psi}_R^S}{dt} - jp\omega_m \boldsymbol{\Psi}_R^S \tag{2}$$

$$\boldsymbol{\Psi}_S^S = L_S \boldsymbol{i}_S^S + L_m \boldsymbol{i}_R^S \tag{3}$$

$$\boldsymbol{\Psi}_R^S = L_m \boldsymbol{i}_S^S + L_R \boldsymbol{i}_R^S \tag{4}$$

The stator current, the rotor speed, and the stator voltage used in the above equations are the sensors feedback signals, and the control process of the IMDs do not properly operate if the measured signals are not correct. The incorrect levels of the measurement system can be classified into the following types: bias, drift, scaling, and total failure [4], as mentioned in Table-1 below, where the bias, drift and scaling belong to a soft-sensor fault group; meanwhile, the complete failure of sensors is seen as a hardware-sensor fault [18]. The faulty sensor signals should be isolated and immediately replaced by estimated values to ensure the IMDs in stable operation.

As shown in Table 1, y(t) represents an actual value of measured signals (or actual measured signals), x(t) is a true value of measured objects, K is an arbitrary constant value. The open-circuit fault is the typical case of the total failure

TABLE 1. Expressions of sensor fault types.

Fault type	Mathematical expression
Bias	y(t) = x(t) + offset
Drift	y(t) = x(t) + offset + K*t
Scaling	y(t) = K*x(t)
Failure	y(t) = K

type, in which the K-coefficient is zero. This case is the most serious fault and needs to be detected as soon as possible. On the other hand, the random pulse noise can occur during the transmission of the feedback signals. This signal failure is less critical and randomly exists within a short time only. Thus, we can apply noise filtering algorithms to solve this problem instead of isolating the measured signals.

B. SENSOR FAULT DIAGNOSIS ALGORITHM

Recently, most drive systems apply the FOC based scheme to separate the stator current space vector into two components, one controlling the rotor flux and the other maintaining the required torque, simultaneously. As a solution to deal with the possibility of losing the feedback sensor signals, an FTC algorithm is integrated into the FOC based control scheme of the IMDs against sensor failures. In this section, an improving diagnosis method is proposed to detect steady-state sensor failures.

Fig. 1 describes the block diagram of the FOC based control structure combined with an FTC function. The FTC block receives the reference voltages $\boldsymbol{u}_{S\alpha}, \boldsymbol{u}_{S\beta}$; current sensor signals $\boldsymbol{i}_a$, $\boldsymbol{i}_c$; and the rotor speed from an encoder ω_{en} to implement the FTC algorithms. The current signals $\boldsymbol{i}_a$, $\boldsymbol{i}_c$ in the [a,b,c] coordinate system can be transformed into the [α, β] coordinate system by the modified Clarke formulas as in (5).

$$\begin{bmatrix} i_{S\alpha} \\ i_{S\beta} \end{bmatrix} = \begin{bmatrix} 1 & 0 \\ \frac{-1}{\sqrt{3}} & \frac{-2}{\sqrt{3}} \end{bmatrix} \begin{bmatrix} i_a \\ i_c \end{bmatrix} \tag{5}$$

The proposed FTC function includes three stages, i.e., fault diagnosis, isolation, and reconfiguration, for both current and speed sensor faults. The proposed FTC principle is described as the block diagram presented in Fig. 2. The FTC outputs include two groups: status indicators and feedback values for the FOC loops. If the drive system is in normal condition, the outputs are the measured rotor speed and the [α, β] components of the measured stator currents. When any sensor fault occurs in either the current sensor or speed sensor, the FTC function immediately detects the faults. Then, corresponding to the reconfiguration step, estimated signals are used as the FTC outputs instead of such faulty sensor signals to ensure the IMD is still working in stable operation. At the same time, the corresponding sensor flag is also issued to inform the exact error type.

Based on the IM model, the estimated stator currents can be determined by applying the modified Luenberger observer [19] (or we can also use some other suitable methods) as

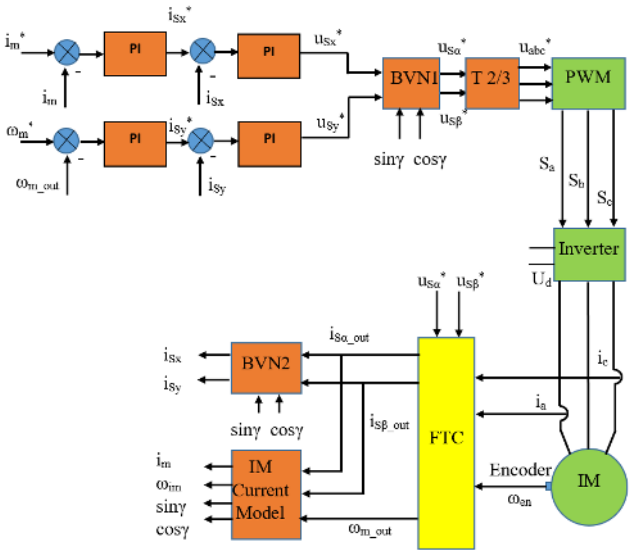

FIGURE 1. FOC based control structure with integrated FTC function for IMDs.

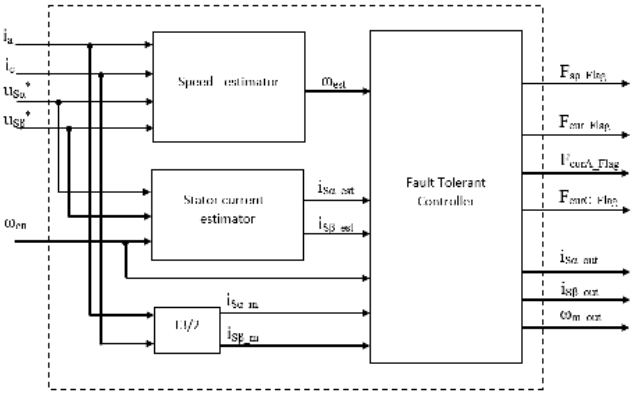

FIGURE 2. Block diagram of FTC unit.

below:

$$\begin{cases} \dot{\hat{x}} = A(\omega_{en})\hat{x} + Bu + L\xi \\ \hat{y} = C\hat{x} \end{cases} \tag{6}$$

where

$$\begin{aligned} \hat{x} &= [i_{S\alpha\_est} \;\; i_{S\beta\_est} \;\; \psi_{R\alpha\_est} \;\; \psi_{R\beta\_est}]^T \\ \hat{y} &= [i_{S\alpha\_est} \;\; i_{S\beta\_est}]^T \\ u &= [u^*_{S\alpha} \;\; u^*_{S\beta}]^T \\ \xi &= [-i_{S\alpha\_est} \;\; -i_{S\beta\_est}]^T \\ L &= \begin{bmatrix} L_1 & L_2 & L_3 & L_4 \\ -L_2 & L_1 & -L_4 & L_3 \end{bmatrix} \end{aligned}$$

The estimated stator current components ($\boldsymbol{i}_{S\alpha\_est}, \boldsymbol{i}_{S\beta\_est}$) in the [$\alpha$, β] coordinate can be obtained from (6) as follows:

$$\begin{aligned} \frac{di_{S\alpha\_est}}{dt} = &-\frac{\left(L_m^2 R_R + L_R^2 R_S\right)}{\sigma L_S L_R^2} i_{S\alpha\_est} + \frac{L_m R_R}{\sigma L_S L_R^2} \psi_{R\alpha\_est} \\ &+ \frac{L_m p \omega_{en}}{\sigma L_S L_R} \psi_{R\beta\_est} + \frac{u^*_{S\alpha}}{\sigma L_S} - L_1 i_{S\alpha\_est} + L_2 i_{S\beta\_est} \end{aligned} \tag{7}$$

$$\frac{di_{S\beta\_est}}{dt} = -\frac{\left(L_m^2 R_R + L_R^2 R_S\right)}{\sigma L_S L_R^2} i_{S\beta\_est} - \frac{L_m p\omega_{en}}{\sigma L_S L_R}\psi_{R\alpha\_est} + \frac{L_m R_R}{\sigma L_S L_R^2}\psi_{R\beta\_est} + \frac{u^*_{S\beta}}{\sigma L_S} - L_2 i_{S\alpha\_est} - L_1 i_{S\beta\_est} \quad (8)$$

$$\frac{d\psi_{R\alpha\_est}}{dt} = \frac{L_m R_R}{L_R} i_{S\alpha\_est} - \frac{R_R}{L_R}\psi_{R\alpha\_est} - p\omega_{en}\psi_{R\beta\_est} - L_3 i_{S\alpha\_est} + L_4 i_{S\beta\_est} \quad (9)$$

$$\frac{d\psi_{R\beta\_est}}{dt} = \frac{L_m R_R}{L_R} i_{S\beta\_est} + p\omega_{en}\psi_{R\alpha\_est} - \frac{R_R}{L_R}\psi_{R\beta\_est} - L_4 i_{S\alpha\_est} + L_3 i_{S\beta\_est} \quad (10)$$

where

$$\begin{aligned}
\sigma &= (1 - \frac{L_m^2}{L_S L_R});\ T_R = \frac{L_R}{R_R};\ T_S = \frac{L_S}{R_S}\\
L_1 &= (k-1)(\frac{1}{\sigma T_S} + \frac{1}{\sigma T_R})\\
L_2 &= -(k-1)p\omega_{en}\\
L_3 &= (k^2-1)\left[(\frac{1}{\sigma T_S} + \frac{1}{\sigma T_R})\frac{\sigma L_S L_m}{L_R} - \frac{L_m}{T_R}\right]\\
L_4 &= -(k-1)\frac{\sigma L_S L_m}{L_R} p\omega_{en};\\
k &> 1;
\end{aligned}$$

If a current sensor fault occurs, the estimated currents will be used to replace the measured currents. In this case, the estimated stator current components in the $[\alpha, \beta]$ coordinates are the FTC outputs.

Similarly, if a speed sensor fault occurs, the reconfiguration is implemented and the measured rotor speed signal is replaced by a value of a speed estimator. The methods based on machine models such as RF-MRAS, EMF-MRAS, and CB-MRAS [20]–[26] are preferred because of their simplicity and good performance. Other structures of speed-sensorless controllers based on variable-structure control theory, e.g., Sliding Mode Observer (SMO) was also proposed in [27]–[31] thanks to their significant advantages, such as less influence by the change of machine parameters, external disturbance rejection, and fast dynamic response [27], [28]. In this paper, the estimated speed method based on SMO is used in the structure of the FTC [28] where the estimated stator currents and the rotor flux can be obtained according to the following equations:

$$\frac{d\hat{\boldsymbol{i}}_S^S}{dt} = -\frac{R_S + (L_m/L_R)^2 R_R}{\sigma L_S}\hat{\boldsymbol{i}}_S^S + \frac{L_m}{\sigma L_S L_R}(\frac{1}{T_R} - j\omega_{est})\boldsymbol{\psi}_R^S + \frac{1}{\sigma L_S}\boldsymbol{u}_S^S + G_1 \mathrm{sat}(\boldsymbol{i}_{S\_m}^S - \hat{\boldsymbol{i}}_S^S) \quad (11)$$

$$\frac{d\hat{\boldsymbol{\psi}}_R^S}{dt} = \frac{L_m}{T_R}\hat{\boldsymbol{i}}_S^S - (\frac{1}{T_R} - j\omega_{est})\hat{\boldsymbol{\psi}}_R^S + G_2 \mathrm{sat}(\boldsymbol{i}_{S\_m}^S - \hat{\boldsymbol{i}}_S^S) \quad (12)$$

$$\omega_{est} = K_P z + K_I \int z \cdot dt \quad (13)$$

$$sat(x) = \begin{cases} 1, & if\ x > \Delta \\ x/\Delta, & if\ |x| < \Delta \\ -1, & if\ x < \Delta \end{cases} \quad (14)$$

where

$$\begin{aligned}
z &= \left(i_{S\alpha_m} - i_{S\alpha_est}\right)\psi_{R\beta_est} - \left(i_{S\beta_m} - i_{S\beta_est}\right)\psi_{R\alpha_est}\\
G_1 &= -(g_{11} + jg_{12});\ G_2 = -(g_{21} + jg_{22})\\
g_{11} &= -\lambda(k-1)(R_S L_R + R_R L_S)\\
g_{12} &= (k-1)\omega_{est}\\
g_{21} &= (k-1)(R_R L_S - kR_S L_R)/\mathrm{L}_m\\
g_{22} &= -(k-1)\omega_{est}/(\lambda L_m)\\
\lambda &= 1/(L_S L_R - L_m^2)\\
\mathrm{k} &> 1;\ \Delta : \text{positive constant}
\end{aligned}$$

This research focuses on modifying the sensor fault diagnosis methods and applying existing sensorless methods published in other referenced papers for the reconfiguration step. Thus, the paper contributions are the proposed approaches to effectively diagnose sensor faults in the Fault Detection Function. The improved diagnosis algorithm reliably detects any faults of the speed sensor and current sensor in IMDs. However, the proposed FTC operation in sensorless mode can deal with a single type of sensor fault only, i.e., either a speed sensor or current sensor fault, not both the speed and current sensors damaged simultaneously. Fig. 3 below shows the flowchart of the fault diagnosis algorithm. It also describes the full functions of the FTC as detecting the fault, isolating wrong signals, and replacing the inaccurate measured values with suitable estimated values. Many fault detection functions combined in the diagnosis algorithm are presented in the flowchart, each of which is used to detect a specific type of the sensor faults. The speed sensor diagnosis is firstly executed by comparing the reference rotor speed and the sensor feedback signal and then confirmed by a counter as a time checking. The speed sensor diagnosis implementation can be described as the following steps:

$$\begin{aligned}
&If(\left|\omega_{ref} - \omega_{en}\right| > Threshold_1)\\
&\{SpF_Counter = SpF_Counter + 1;\}\\
&Else\\
&\{SpF_Counter = 0;\}\\
&If(SpF_Counter \geq Sp_Coe)\\
&\{F_{sp_Flag} = 1;\}
\end{aligned} \quad (15)$$

Threshold_1 depends on the range of the rotor speeds [6], as defined by

$$Threshold\_1 = \begin{cases} 0.045 * \left|\omega_{ref}\right|; \text{if rotor-speed} > 200\,\text{rpm} \\ 0.1 * \left|\omega_{ref}\right|; \text{if rotor-speed} \leq 200\,\text{rpm} \end{cases}$$

Sp_Coe is a setting value for the speed sensor fault detection

In this research, practical experiments have been performed using a TMS320F28335-based control system, where an Analog-to-Digital Converter (ADC) processing cycle is

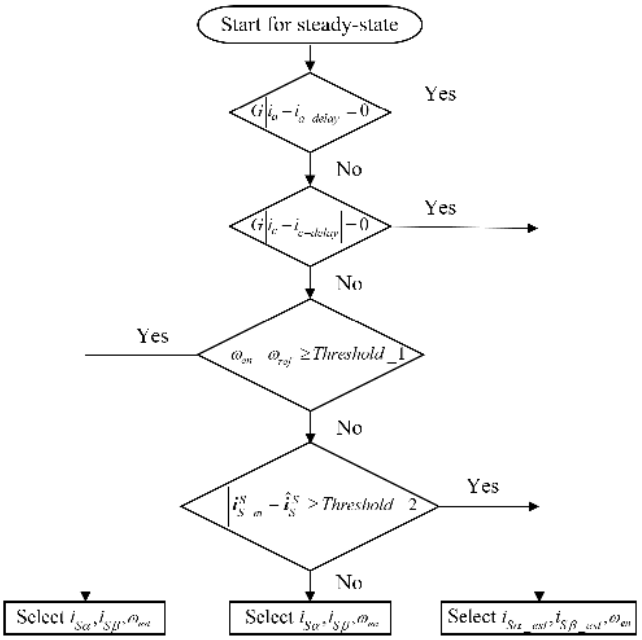

FIGURE 3. Flowchart of proposed FTC algorithm.

set to 100 μs (as a sampling cycle). The duration to ensure reliable faults is assigned as $Sp\_Coe = 30$ (a threshold of the speed counter), which is the multiple of 100 μs. As observed from the various practical experiments, most random pulse noises occur in a very short time, less than 20 ADC-cycles, thus selecting Sp_Coe of 30 sampling cycles is sufficient to ignore unexpected pulse noises and make the execution time for the speed sensor fault detection very fast, about 3 ms.

The stator current sensor diagnosis is executed at the next step by comparing the amplitudes of the measured and estimated current space vectors defined by

$$\boldsymbol{i}_{S\_m}^{S} = \sqrt{i_{S\alpha\_m}^2 + i_{S\beta\_m}^2};\ \hat{\boldsymbol{i}}_{S}^{S} = \sqrt{i_{S\alpha\_est}^2 + i_{S\beta\_est}^2} \tag{16}$$

The implementation can be described by the following steps:

$$\begin{aligned} &If(\left|\left|\boldsymbol{i}_{S\_m}^{S}\right| - \left|\hat{\boldsymbol{i}}_{S}^{S}\right|\right| \geq Threshold\_2) \\ &\{CurF\_Counter = CurF\_Counter + 1;\} \\ &Else\{Cur\_Counter = 0;\} \\ &If((F_{sp\_Flag} = 0)\&\&(Cur\_Counter \geq Cur\_Coe)) \\ &\{F_{cur\_Flag} = 1;\} \end{aligned} \tag{17}$$

where Cur_Coe is a set time of a current counter, which is used to avoid random pulse noises and discriminate between the speed sensor and current sensor faults.

$Threshold\_2$ is a limit deviation between the measured and estimated current space vectors in normal conditions. According to the various practical experiments, we propose an appropriate deviation of 10% of the rated current for $Threshold\_2$.

In fact, the estimated current space vector is derived from the speed sensor signal according to (7), (8), (9), and (10).

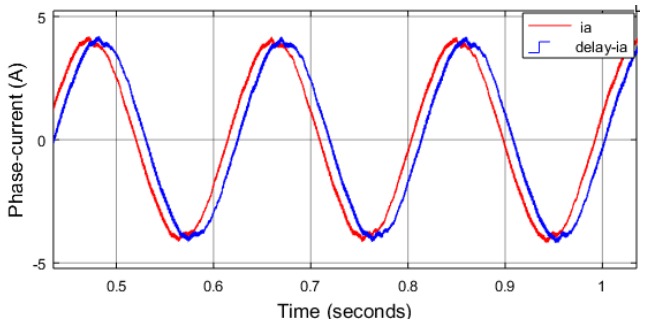

FIGURE 4. A phase current signal and its delayed-signal.

If the speed sensor fails the estimated currents are inaccurate and it can lead to misunderstanding between the speed sensor and current sensor fault detection. To solve this problem, the set time of the current counter Cur_Coe must be longer than that of the speed counter Sp_Coe. In this research, we have chosen a value of 35 sampling cycles (3.5 ms) for Cur_Coe. As a result, it prevents the confusion between the speed sensor and current sensor faults for any speed sensor failures. In other words, the FTC needs a specific delay time to precisely recognize the existence and type of the sensor faults.

Moreover, in a severe case where the current sensor signals are totally lost, it is necessary to immediately detect the fault and switch to the sensorless mode. To solve this circumstance, we propose a new approach called a delay algorithm to detect the lost signals of the current sensors. The main idea of the proposed delay method comes from many practical experiments where the sinusoidal phase current signal and its delayed signal, which are both measured by the current sensors, are compared together. Suppose at t = 0; an instantaneous current value measured by the current sensor is read and the data is stored in a variable called Cur_t0. Then, at t = 100 μs (one next cycle of the ADC interrupt), another instantaneous current value is read and stored in a variable Cur_t1. Therefore, at this time, Cur_t1 is the present value of the sinusoidal phase current, and Cur_t0 is the value of its delayed signal. In normal conditions, at any time, the value of Cur_t1 is always different from the value of Cur_t0, as shown in Fig. 4.

If a total current sensor fault occurs, the measured signal is completely lost. As a result, all current sensor signals become zero and all stored present and delayed signals are also zero ($Cur\_t0 = Cur\_t1 = Cur\_t2 = ... = Cur\_tn = 0$); or in some cases they keep a constant value as mentioned in [18]. It means that a total fault of the current sensors lead to similar values between the present and delayed current signals. It is evaluated using (18).

$$\begin{aligned} &Index\_I_j = G * \left|i_j - i_{delay\_j}\right| \\ &\text{where:} \\ &\text{“j”: the phase of stator current.} \\ &\text{“G”: the gain coefficient.} \end{aligned} \tag{18}$$

The deviation of the present signals and its delayed signals is very small. Therefore, we need to amplify this deviation so the fault detection program is more comfortable and more stable. This coefficient is not too important and it can be calculated from the sine-function ($i(t) = I_m.\sin(\omega.\Delta t)$; $\Delta t = 100\ \mu s$), but using the experimental tests is simpler. Indeed, we have implemented through the trial-and-error way from various experiments to find it. A value greater than 8 usually adopt a general requirement for the fault detection algorithm, so we decided to choose G = 10 for more convenience. The loss of the current sensors is detected by the following steps:

$$\begin{aligned} &If\,(Index\_I_j = 0)\\ &\{CurF\_Counter_j = CurF\_Counter_j + 1;\}\\ &If\,(CurF\_Counter_j \geq Cur_j\_Coe)\\ &\{F_{curj\_Flag} = 1;\}\\ &If\,(F_{curj\_Flag} = 1)\\ &\{F_{cur\_Flag} = 1;\} \end{aligned} \tag{19}$$

where

Curj_Coe is a setting for the phase current fault detection

Curj_Coe is set to a value of 20 sampling cycles (2 ms only) to quickly detect the total current fault. Moreover, in a typical structure of IMDs, two current sensors are mostly used, thus the delay algorithm is implemented for two-phase currents.

Finally, the proposed general FTC diagnosis algorithm consists of the various diagnosis elements, each of them is used to detect a specific type of the sensor faults. Table 2 shows the indication codes and corresponding outputs of the proposed diagnosis algorithm, which uses comparators of simple signals only to detect the speed and current sensor faults. Therefore the presented algorithm is simpler and faster than other existing diagnosis methods, which use complicated observers in various coordinate systems. For example, to detect the total loss of the current sensors, most existing methods [14], [16] have implemented comparison functions based on the RMS value of the sine wave signals. Such methodology needs the calculation time at least a half-cycle of the sine-wave currents or more, which is at least 10 ms for the stator frequency of 50 Hz. In the case of the proposed fault detection method, the calculation time takes 2 ms only for the same operating conditions. For low-speed operation, the calculation time of mentioned RMS-based methods correspondingly increases. Thus, the existing fault detection methods could increase IM damage probability due to the longer time in the problem-solving. On the other hand, we can optimize the costs of the computational hardware system due to the low calculation burden of the proposed algorithm.

III. SIMULATION RESULTS

In this section, many simulations have been implemented to demonstrate the proposed FTC approach with various insufficient cases in IMD measurement systems. Normally, the speed sensorless control schemes often have operational difficulties in a low-speed range (10% of the rated speed) due to the sensitivity of machine parameters and nonlinearity of inverters. Thus, the simulations have been implemented in the low-speed region, where the operating motor speed is set to 10% of the rated value under three sensor fault types:

- Speed sensor fault.
- Scaling-defect of current sensors.
- Total-failure of current sensors.

The structure of the IMD measurement system consists of two current sensors and a speed sensor, as shown in Fig. 1. The machine parameters are listed in Table 3.

The operation condition of the IMD is specified by a speed ramping up from zero to 10% of the rating value (150 rpm) at the time from zero to 0.1 s and then keeping as a constant, as shown in Fig. 5. The following parts introduce the performance of the proposed FTC unit under these three sensor fault types.

In the first simulation, the induction motor operates in normal speed characteristics, as shown in Fig. 5, but sudden damage of the speed sensor happens at 2.0 s. Thus, the measured sensor signal is lost, and the controller feedback signal receives zero value. At that moment, the speed sensor diagnosis algorithm determines the difference between the reference rotor speed and the sensor feedback signal, and it quickly detects this problem after 30 sample pulse cycles. The speed sensor diagnosis algorithm execution can be seen in (15) of the previous section. Then, the estimated rotor

TABLE 2. Judgment principle of FTC function.

Fault code	Diagnosis result
F_{sp_Flag}=0, F_{cur_Flag}=0, F_{curA_Flag}=0, F_{curC_Flag}=0	Healthy
F_{sp_Flag}=1, F_{cur_Flag}=0, F_{curA_Flag}=0, F_{curC_Flag}=0	Speed sensor fault
F_{sp_Flag}=0, F_{cur_Flag}=1, F_{curA_Flag}=0, F_{curC_Flag}=0	Current sensor fault
F_{sp_Flag}=0, F_{cur_Flag}=1, F_{curA_Flag}=1, F_{curC_Flag}=0	Total sensor fault of A phase
F_{sp_Flag}=0, F_{cur_Flag}=1, F_{curA_Flag}=, F_{curC_Flag}=1	Total sensor fault of C phase

TABLE 3. Motor parameters.

Symbol	Quantity	Value (unit)
P_n	Rated Power	2.2 (kW)
U_n	Rated Voltage	400 (V)
ω_n	Rated speed	1420 (rpm)
I_S	Rated stator current	4.85 (A)
R_S	Stator resistance	3.179 (Ω)
R_R	Rotor resistance	2.118 (Ω)
L_m	Mutual inductance	0.192 (H)
J	Moment of inertia	0.047 (Kgm^2)
p	Pole pair number	2
L_S	Stator inductance	0.209 (H)
L_R	Rotor inductance	0.209 (H)
Ψ_{Sn}	Rated Rotor flux	0.757 (Wb)

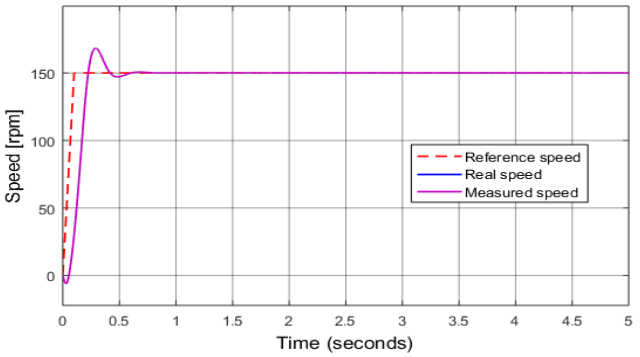

FIGURE 5. Reference, real, and measured rotor speed.

speed is used to replace the lost measured signal. As a result, the IMD keeps stable operation under the speed sensor fault stage, as shown in Fig. 6. Moreover, the FTC is described as part (c) of Fig. 6, where only the speed sensor-flag is changed, and other indicators corresponding to the different sensor types remain.

In the next simulation, suppose that a scaling current sensor defect in phase A occurs at the time of 2.0 s, and the measured values of normal and suffered sensors are significantly different, as shown in Fig. 7 part (a). At that moment, the current sensor diagnosis algorithm based on (17) quickly detects the current sensor failure after 35 sample pulse cycles. The FTC unit then replaces all the measured signals with the estimated currents for the FOC controllers, as shown in Fig. 7 (b). The IMD operating speed is presented in Fig. 7 part (c), where the motor speed is just fluctuated slightly in a short time and then quickly stabilized again. Fig. 7 part (d) demonstrates the high performance of the proposed diagnosis algorithm in accurately detecting the fault type. Only the current sensor fault flag is activated to indicate an error in one of the current sensors but not the total broken failure.

Similarly, the last simulation describes the total current sensor failure that occurrs at 2.0 s in phase C. Hence, the measured current signal in phase C is lost as shown in Fig. 8 part (a), and the comparison between the phase C current and its delayed signal becomes zero value because both values reach zero. This diagnosis algorithm execution is presented in (18) and (19) of the previous section. In this case, the critical sensor fault is quickly solved by the FTC unit within 20 sample pulse cycles only. In particular, the estimated currents of both two phases A and C are used as the FTC current outputs to replace the lost measured signal in phase C and the normally measured signal in phase A. It makes the response of the FTC for this problem faster and simpler. Fig. 8 part (c) presents the IMD operation in this situation where the speed characteristics are maintained stably even in the fault-tolerant modes due to promptly and precisely reacting to the FTC. As a result, we nearly do not see any oscillations of the IMD during the operation.

Furthermore, as shown in Fig. 8 part (d), the diagnosis algorithm exactly detects the faulty current sensor failure type and position by issued two flags, i.e., the total broken

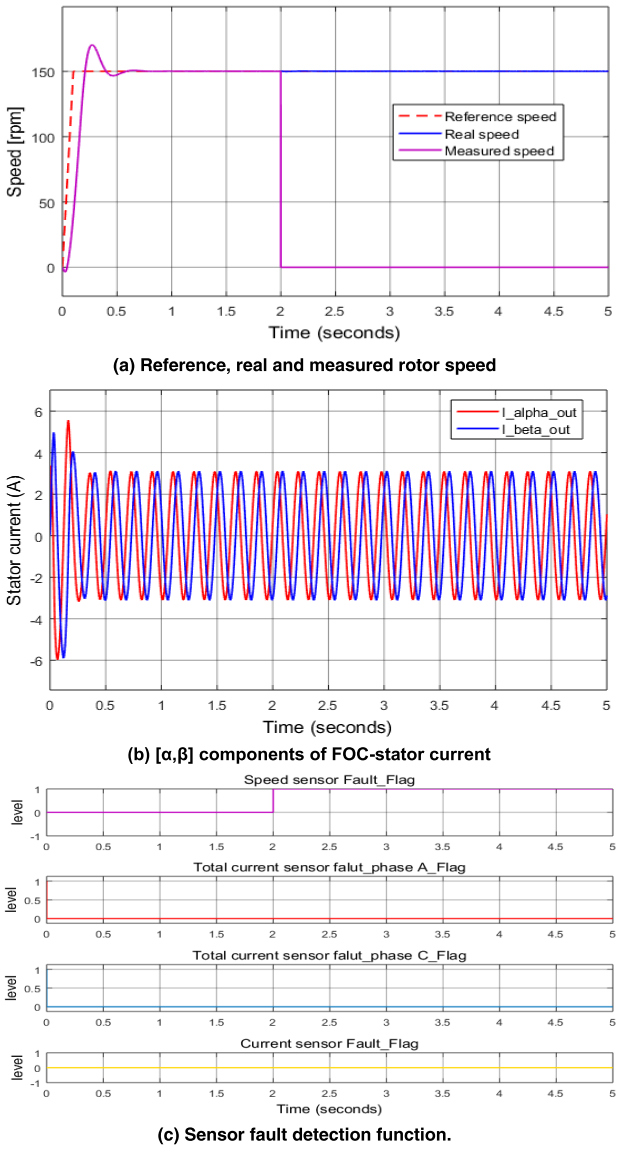

FIGURE 6. Simulation results - Speed sensor fault – FTC.

failure in phase C and the general failure of the current sensors. It implies that if and only if the general failure of the current sensors and one of the total broken failure flags are simultaneously activated, the FTC sets the total broken failure mode.

Finally, according to the three simulation-based experiments above, the proposed FTC unit has proved the high performance in effectively dealing with various insufficient cases of the measuring system of the IMD. It can especially work well in a low-speed zone, which causes the complication in the electromagnetic transferring process of IMDs.

IV. EXPERIMENTAL RESULTS

The practical experiments have been set up and implemented in real devices at our Intelligent Motor Control Lab to evaluate the proposed FTC method ability in practice.

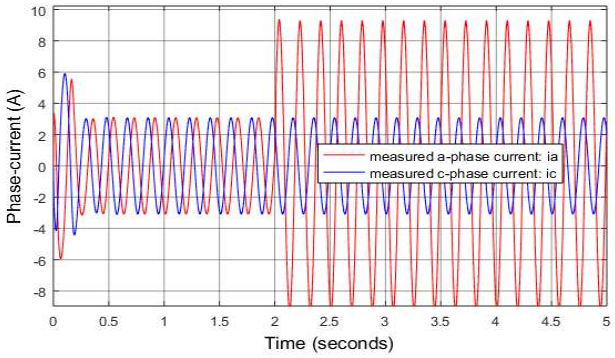

(a) Measured current

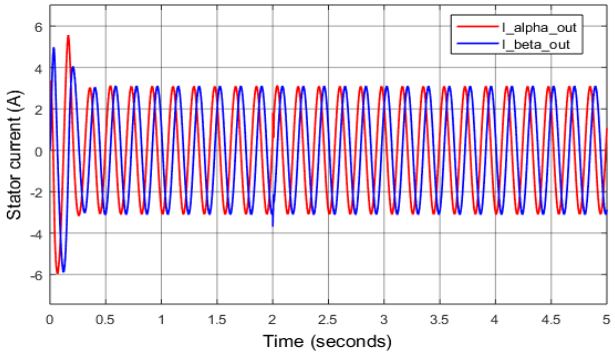

(b) [α,β] components of FOC-stator current

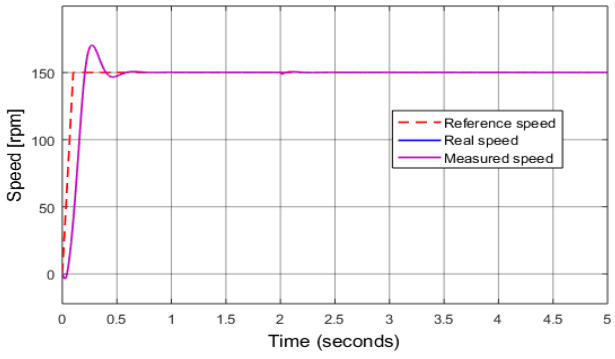

(c) Reference, real and measured rotor speed

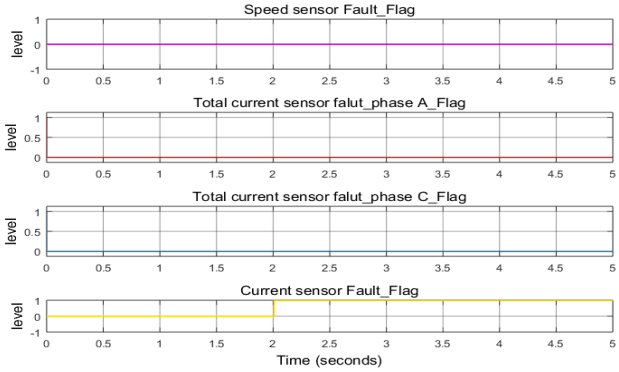

(d) Current fault detection function

FIGURE 7. Simulation results – Scaling current sensor fault – FTC.

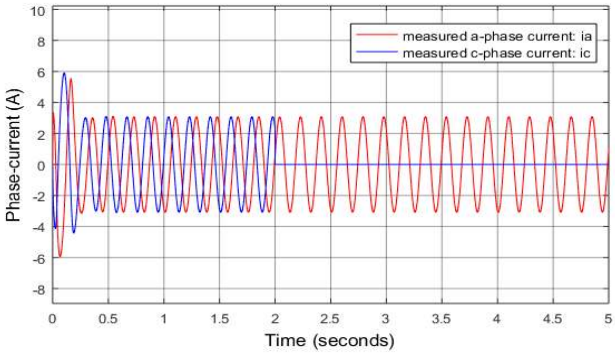

(a) Measured current

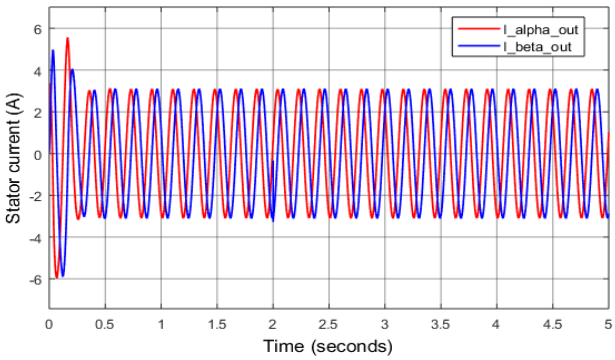

(b) [α,β] components of FOC-stator current

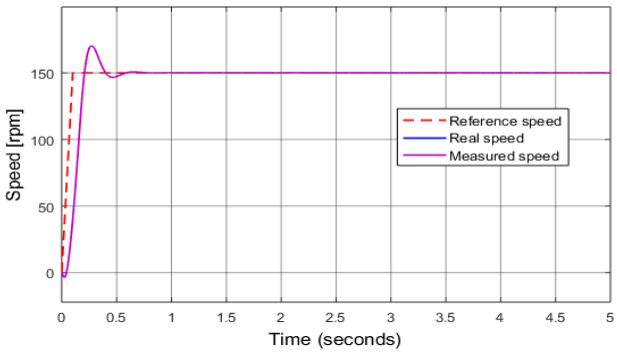

(c) Reference, real and measured rotor speed

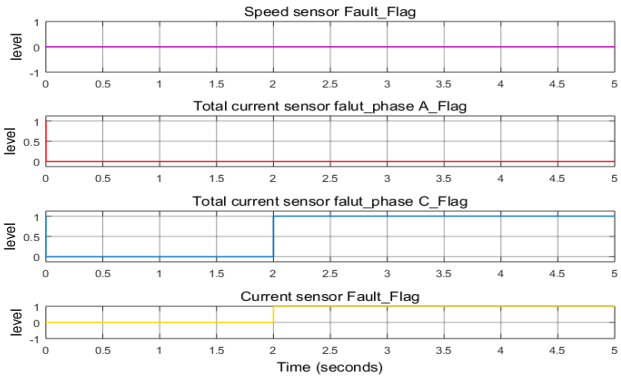

(d) Current fault detection function

FIGURE 8. Simulation results – Total current sensor fault – FTC.

The experimental structure (hardware) includes an induction motor, a controllable load, an inverter controlled by the TMS320F28335-DSP, and a three-phase power supply. The control algorithms (software) are developed by the C++ programming language in Code Composer Studio (CCS) programming environment. Fig. 9 shows the whole laboratory system.

The experiments have also been implemented in the same scenarios as the simulations mentioned in the previous section

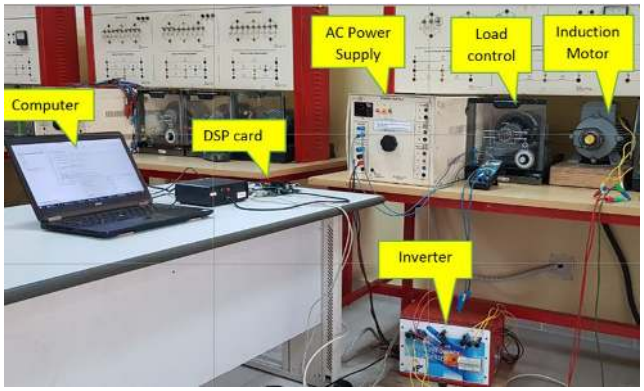

FIGURE 9. Laboratory stand.

to investigate the correlation between the simulation and experimental results. Thus, the experiments have considered the three sensor fault types: speed sensor fault, scaling defect of the current sensors, and total failure of the current sensors at the low-speed region where the operating motor speed is set to 150 rpm, i.e., 10% of the rated speed value. The operation condition of the IMD is specified by a speed ramping up from zero to 150 rpm at the time from zero to 0.1 s and then keeping as a constant.

In the first experiment, as shown in Fig. 10 part (a), from zero to 2.0 s, the induction motor operates in normal conditions. However, at the time of 2.0 s, sudden damage of the speed sensor occurs. Thus, the measured speed sensor signal is lost, and the controller feedback signal receives zero value. At that moment, the speed sensor diagnosis algorithm determines the difference between the reference rotor speed and the sensor feedback signal, and it quickly determines this problem after 30 sample pulse cycles. Due to the processing cycle of the DSP set to 100 μs, the diagnosis algorithm execution time is correspondingly about 3 ms. The estimated rotor speed is then used to replace the lost measured signal, and the IMD operates under the FTC mode afterward. As we can see in Fig. 10, part (a), the actual speed characteristics still keep stable operation. However, it seems not to be as good as the regular operation with an appropriate speed sensor signal.

Similar to the simulation result, the speed sensor-flag is activated only, and other error indicators corresponding to the different sensor types remain as described in part (c) of Fig. 10.

Fig. 11 describes the FTC operation against the current sensor failure where a scaling defect is considered in the measured value of phase A at t = 2 s while phase C is appropriate. At that moment, the current sensor diagnosis algorithm quickly detects the problem of the current sensor failure after 35 sample pulse cycles. This delay time is set later than that of the speed sensor diagnosis algorithm to prevent confusion between these two cases. Due to the processing cycle of TMS320F28335 set to 100 μs, the current sensor failure flag is correspondingly issued about 3.5 ms. The FTC unit replaces the measured signals, both phases A and C, with the estimated currents to the FOC controllers, as shown in

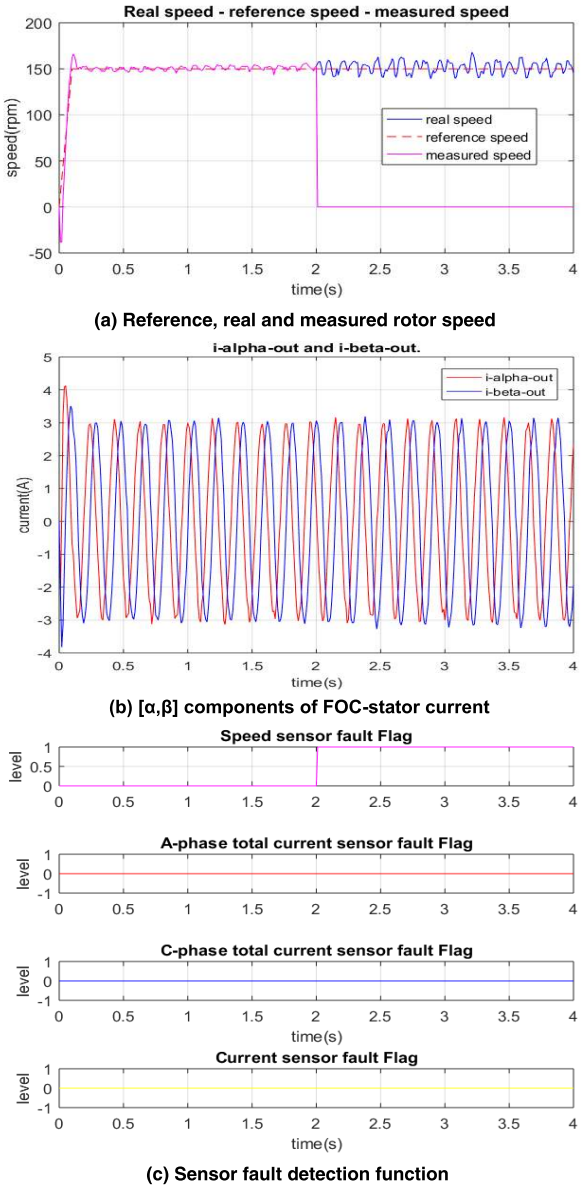

FIGURE 10. Experimental results - Speed sensor fault - FTC.

Fig. 11 (b). It makes the response of the FTC for this problem faster and simpler. The motor speed characteristics under the FTC mode are presented in Fig. 11, part (c). After t = 2 s, the motor speed remains stable, similar to the normal mode with appropriate current sensors. Moreover, as shown in Fig. 11 part (d), only the general current sensor fault flag is activated to indicate a defect in one of the current sensors but not the total broken failure or the speed sensor fault.

The last experiment considers the total current sensor failure that occurrs at 2.0 s in phase C. The measured current signal in phase C is lost as shown in Fig. 12 part (a), and the comparison between the phase C current and its delayed signal becomes zero value because both values reach zero. Because this is a critical problem, the diagnosis algorithm quickly determines the exact failure type and set the FTC

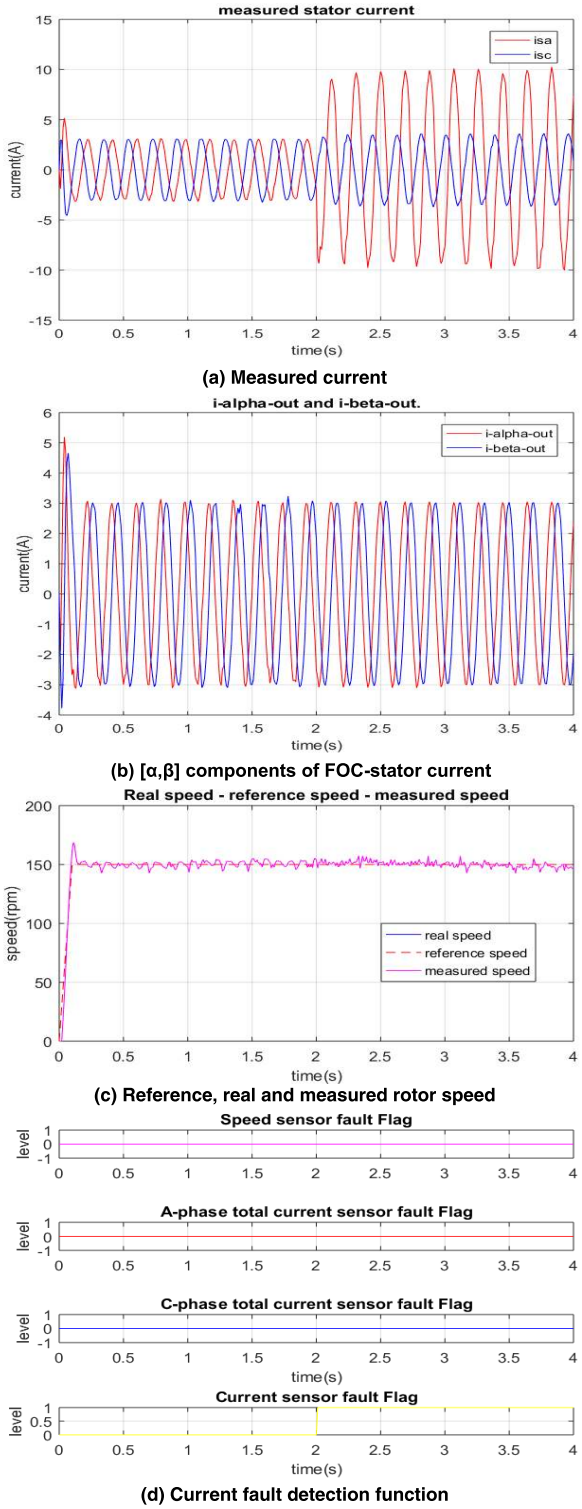

FIGURE 11. Experimental results – Scaling current sensor fault – FTC.

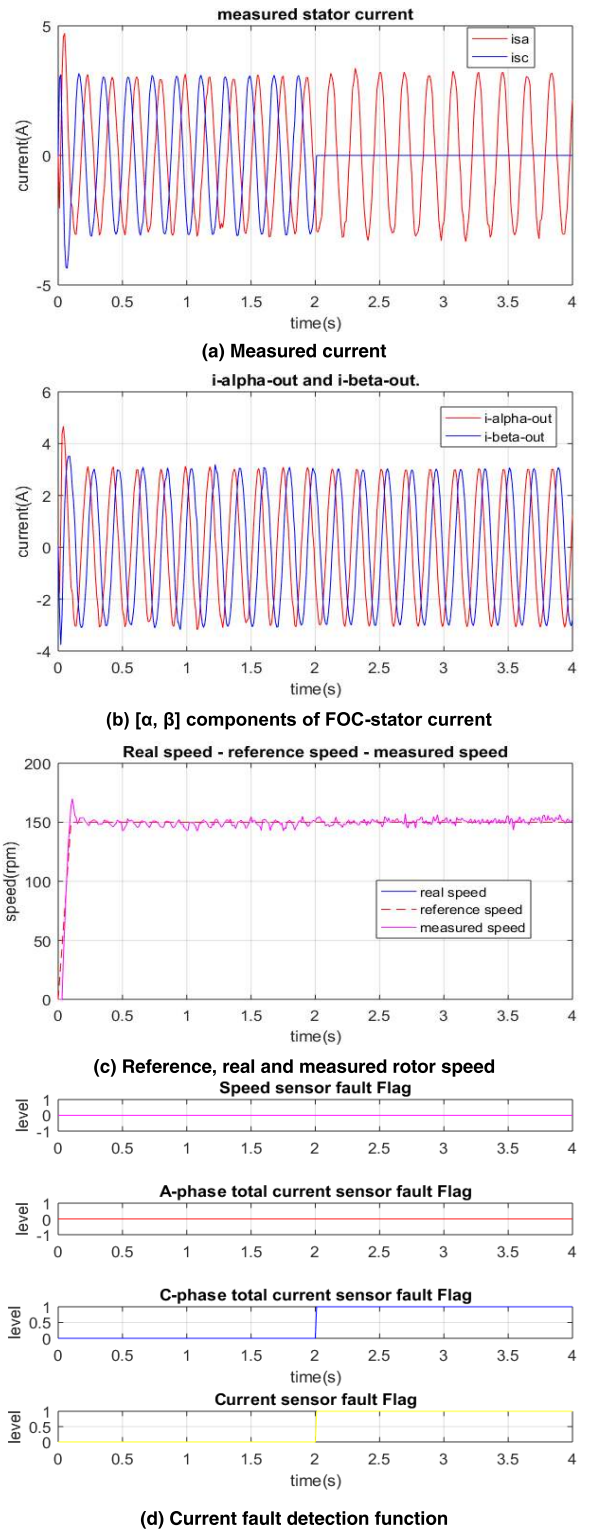

FIGURE 12. Experimental results – Total current sensor fault – FTC.

mode within 20 sample pulse cycles, i.e., 2.0 ms. Like the previous experiment, as shown in Fig. 12 part (b), the estimated currents of both phases A and C are used as the current outputs of the FTC to replace the lost measured signals in phase C and the healthy measured signal in phase A. Fig. 12 part (c) presents the experimental results of the rotor speed characteristic during the transition from the normal to the fault-tolerant mode. Similar to the same simulation scenario, the diagnosis algorithm precisely detects the faulty current sensor failure type and position by issued two flags, the total

broken failure in phase C and the general failure of the current sensors.

Therefore, according to the experiments in the real IMD system, we can see the proposed FTC high performance against various insufficient measuring system cases in practice.

In fact, the proposed FTC has been developed to deal with both speed and current sensor failures. However, the proposed approach is designed for a single type of the sensor fault occurring at a time, not both the speed and current sensor damaged simultaneously. The reason is coming from practice, the probability of both the speed sensor and the current sensor failures at the same time is too low. Moreover, most induction motor drives are manufactured with the full sensors, and if a sensor fault occurs, a FTC temporarily switches to a sensorless mode. In general, the FOC performance with sensors is always better than any sensorless method, which is convenient because of reducing the cost, hardware complexity etc. as well as a backup method when a sensor is damaged. Especially, the speed sensorless control schemes often have operational difficulties in a low-speed range (10% of the rated speed and less) due to the sensitivity of machine parameters, the nonlinearity of inverters etc. The IMDs should not generally operate with the faulty sensor for a long time and the broken sensor should be repaired or replaced soon to recover normal operation. As demonstrated by both the simulations and experiments, the proposed FTC approach can stably work if the speed sensor is damaged, but two current sensors are still healthy. Similarly, even when all of the two current sensors are broken, it also works stably if the speed sensor is good. But, in a special case when both the speed sensor and any current sensor are simultaneously faulty, the proposed FTC approach cannot operate stably.

V. CONCLUSION

This paper presents a novel diagnosis method for the speed and current sensor fault-tolerant control of induction motor drives. The proposed method has proven its effectiveness in dealing with multi-type sensor failures. The speed sensor fault diagnosis algorithm can reliably detect the inaccuracy of the speed sensor signals without interference by random pulse noises. The loss of the current sensor signals, which is the most severe current sensor fault, is quickly detected by the delay-algorithm. Other types of current sensor failures is reliably identified without misunderstanding with a speed sensor fault. The proposed diagnosis algorithm is simpler than other existing detection methods, and thus, the computational hardware system executes faster as well as cheaper due to the lower calculation burden for the same operating conditions. The simulation and experimental results have demonstrated the efficiency of the proposed method. Further research can be implemented to improve the diagnosis of the sensor faults in transient states.

REFERENCES

[1] T. F. Chan and K. Shi, *Applied Intelligent Control of Induction Motor Drives*, 1st ed. Hoboken, NJ, USA: Wiley, 2011, pp. 1–7.

[2] A. Gouichiche, A. Safa, A. Chibani, and M. Tadjine, "Global fault-tolerant control approach for vector control of an induction motor," *Int. Trans. Electr. Energy Syst.*, vol. 30, no. 8, Aug. 2020, Art. no. e12440, doi: 10.1002/2050-7038.12440.

[3] D. Diallo, M. E. H. Benbouzid, and M. A. Masrur, "Special section on condition monitoring and fault accommodation in electric and hybrid propulsion systems," *IEEE Trans. Veh. Technol.*, vol. 62, no. 3, pp. 962–964, Mar. 2013, doi: 10.1109/TVT.2013.2245731.

[4] A. A. Amin and K. M. Hasan, "A review of fault tolerant control systems: Advancements and applications," *Measurement*, vol. 143, pp. 58–68, Sep. 2019, doi: 10.1016/j.measurement.2019.04.083.

[5] A. Raisemche, M. Boukhnifer, C. Larouci, and D. Diallo, "Two active fault-tolerant control schemes of induction-motor drive in EV or HEV," *IEEE Trans. Veh. Technol.*, vol. 63, no. 1, pp. 19–29, Jan. 2014, doi: 10.1109/TVT.2013.2272182.

[6] Y. Azzoug, A. Menacer, R. Pusca, R. Romary, T. Ameid, and A. Ammar, "Fault tolerant control for speed sensor failure in induction motor drive based on direct torque control and adaptive stator flux observer," in *Proc. Int. Conf. Appl. Theor. Electr. (ICATE)*, Oct. 2018, pp. 1–6.

[7] B. Tabbache, M. E. H. Benbouzid, A. Kheloui, and J.-M. Bourgeot, "Virtual-sensor-based maximum-likelihood voting approach for fault-tolerant control of electric vehicle powertrains," *IEEE Trans. Veh. Technol.*, vol. 62, no. 3, pp. 1075–1083, Mar. 2013, doi: 10.1109/TVT.2012.2230200.

[8] C. D. Tran, P. Brandstetter, M. C. H. Nguyen, S. D. Ho, B. H. Dinh, and P. N. Pham, "A robust diagnosis method for speed sensor fault based on stator currents in the RFOC induction motor drive," *Int. J. Electr. Comput. Eng.*, vol. 10, no. 3, pp. 3035–3046, Jun. 2020, doi: 10.11591/ijece.v10i3.pp3035-3046.

[9] D. L. Mon-Nzongo, T. Jin, G. Ekemb, and L. Bitjoka, "Decoupling network of field-oriented control in variable-frequency drives," *IEEE Trans. Ind. Electron.*, vol. 64, no. 7, pp. 5746–5750, Jul. 2017, doi: 10.1109/TIE.2017.2674614.

[10] G.-J. Jo and J.-W. Choi, "Gopinath model-based voltage model flux observer design for field-oriented control of induction motor," *IEEE Trans. Power Electron.*, vol. 34, no. 5, pp. 4581–4592, May 2019, doi: 10.1109/TPEL.2018.2864322.

[11] J. R. Dominguez, I. Duenas, and S. Ortega-Cisneros, "Discrete-time modeling and control based on field orientation for induction motors," *IEEE Trans. Power Electron.*, vol. 35, no. 8, pp. 8779–8793, Aug. 2020, doi: 10.1109/TPEL.2020.2965632.

[12] Y. Yu, Y. Zhao, B. Wang, X. Huang, and D. Xu, "Current sensor fault diagnosis and tolerant control for VSI-based induction motor drives," *IEEE Trans. Power Electron.*, vol. 33, no. 5, pp. 4238–4248, May 2018, doi: 10.1109/TPEL.2017.2713482.

[13] C. D. Tran, P. Brandstetter, M. Kuchar, and S. D. Ho, "A novel speed and current sensor fault-tolerant control based on estimated stator currents in induction motor drives," *Int. Rev. Electr. Eng.*, vol. 15, no. 5, pp. 344–351, 2020, doi: 10.15866/iree.v15i5.17937.

[14] T. A. Najafabadi, F. R. Salmasi, and P. Jabehdar-Maralani, "Detection and isolation of speed-, DC-link Voltage-, and current-sensor faults based on an adaptive observer in induction-motor drives," *IEEE Trans. Ind. Electron.*, vol. 58, no. 5, pp. 1662–1672, May 2011, doi: 10.1109/TIE.2010.2055775.

[15] C. Chakraborty and V. Verma, "Speed and current sensor fault detection and isolation technique for induction motor drive using axes transformation," *IEEE Trans. Ind. Electron.*, vol. 62, no. 3, pp. 1943–1954, Mar. 2015, doi: 10.1109/TIE.2014.2345337.

[16] F. R. Salmasi, "A self-healing induction motor drive with model free sensor tampering and sensor fault detection, isolation, and compensation," *IEEE Trans. Ind. Electron.*, vol. 64, no. 8, pp. 6105–6115, Aug. 2017, doi: 10.1109/TIE.2017.2682035.

[17] T. Kikuchi, Y. Matsumoto, and A. Chiba, "Fast initial speed estimation for induction motors in the low-speed range," *IEEE Trans. Ind. Appl.*, vol. 54, no. 4, pp. 3415–3425, Jul. 2018, doi: 10.1109/TIA.2018.2825292.

[18] T.-H. Yi, H.-B. Huang, and H.-N. Li, "Development of sensor validation methodologies for structural health monitoring: A comprehensive review," *Measurement*, vol. 109, pp. 200–214, Oct. 2017, doi: 10.1016/j.measurement.2017.05.064.

[19] Y. Azzoug, R. Pusca, M. Sahraoui, A. Ammar, R. Romary, and A. J. M. Cardoso, "A single observer for currents estimation in sensor's fault-tolerant control of induction motor drives," in *Proc. Int. Conf. Appl. Autom. Ind. Diag. (ICAAID)*, vol. 1, Sep. 2019, pp. 1–6.

[20] P. Brandstetter, "Sensorless control of induction motor using modified MRAS," *Int. Rev. Elect. Eng.*, vol. 7, no. 3, pp. 4404–4411, Jun. 2012.

[21] Y. B. Zbede, S. M. Gadoue, and D. J. Atkinson, "Model predictive MRAS estimator for sensorless induction motor drives," *IEEE Trans. Ind. Electron.*, vol. 63, no. 6, pp. 3511–3521, Jun. 2016, doi: 10.1109/TIE.2016.2521721.
[22] A. Pal, S. Das, and A. K. Chattopadhyay, "An improved rotor flux space vector based MRAS for field-oriented control of induction motor drives," *IEEE Trans. Power Electron.*, vol. 33, no. 6, pp. 5131–5141, Jun. 2018, doi: 10.1109/TPEL.2017.2657648.
[23] S. A. Davari, F. Wang, and R. M. Kennel, "Robust deadbeat control of an induction motor by stable MRAS speed and stator estimation," *IEEE Trans. Ind. Informat.*, vol. 14, no. 1, pp. 200–209, Jan. 2018, doi: 10.1109/TII.2017.2756900.
[24] P. Cao, X. Zhang, S. Yang, Z. Xie, and Y. Zhang, "Reactive-power-based MRAS for online rotor time constant estimation in induction motor drives," *IEEE Trans. Power Electron.*, vol. 33, no. 12, pp. 10835–10845, Dec. 2018, doi: 10.1109/TPEL.2018.2800010.
[25] E. Zerdali and E. C. Menguc, "Novel complex-valued stator current-based MRAS estimators with different adaptation mechanisms," *IEEE Trans. Instrum. Meas.*, vol. 68, no. 10, pp. 3793–3795, Oct. 2019, doi: 10.1109/TIM.2019.2932161.
[26] M. Korzonek, G. Tarchala, and T. Orlowska-Kowalska, "Simple stability enhancement method for stator current error-based MRAS-type speed estimator for induction motor," *IEEE Trans. Ind. Electron.*, vol. 67, no. 7, pp. 5854–5866, Jul. 2020, doi: 10.1109/TIE.2019.2960726.
[27] M. S. Zaky, M. K. Metwaly, H. Z. Azazi, and S. A. Deraz, "A new adaptive SMO for speed estimation of sensorless induction motor drives at zero and very low frequencies," *IEEE Trans. Ind. Electron.*, vol. 65, no. 9, pp. 6901–6911, Sep. 2018, doi: 10.1109/TIE.2018.2793206.
[28] C. Dong, P. Brandstetter, H. H. Vo, and V. H. Duy, "Sliding mode observer for induction motor control," in *AETA 2015: Recent Advances in Electrical Engineering and Related Sciences*. Cham, Switzerland: Springer, 2016, pp. 313–323.
[29] Z. Zhang, H. Liang, C. Wu, and C. K. Ahn, "Adaptive event-triggered output feedback fuzzy control for nonlinear networked systems with packet dropouts and actuator failure," *IEEE Trans. Fuzzy Syst.*, vol. 27, no. 9, pp. 1793–1806, Sep. 2019, doi: 10.1109/TFUZZ.2019.2891236.
[30] M. Morawiec and A. Lewicki, "Application of sliding switching functions in backstepping based speed observer of induction machine," *IEEE Trans. Ind. Electron.*, vol. 67, no. 7, pp. 5843–5853, Jul. 2020, doi: 10.1109/TIE.2019.2914645.
[31] Y. Zhang, Z. Yin, Y. Zhang, J. Liu, and X. Tong, "A novel sliding mode observer with optimized constant rate reaching law for sensorless control of induction motor," *IEEE Trans. Ind. Electron.*, vol. 67, no. 7, pp. 5867–5878, Jul. 2020, doi: 10.1109/TIE.2019.2942577.

CUONG DINH TRAN was born in Ho Chi Minh City, Vietnam, in 1982. He received the M.E. degree from the Ho Chi Minh City University of Technology, Vietnam, in 2008, and the Ph.D. degree in electrical engineering from the VSB-Technical University of Ostrava, Czech Republic, in 2020. He is currently a Lecturer with the Department of Electrical and Electronics Engineering, Ton Duc Thang University, Ho Chi Minh City. His research interests include application of modern control methods and intelligent algorithms in induction motor drives.

PETR PALACKY was born in Novy Jicin, Czech Republic, in 1970. He received the M.Sc. and Ph.D. degrees in electrical engineering from the VSB-Technical University of Ostrava, Czech Republic, in 1993 and 2000, respectively. He is currently an Associate Professor in electrical machines, apparatus and drives and the Head of the Department of Electronics, Faculty of Electrical Engineering and Computer Science, VSB-Technical University of Ostrava. His research interests include microcomputer control systems, modern control methods of ac drives, and machine parameters identifications.

MARTIN KUCHAR was born in Ostrava, Czech Republic, in 1977. He received the M.Sc. and Ph.D. degrees in electrical engineering from the VSB-Technical University of Ostrava, Czech Republic, in 2000 and 2003, respectively. He worked as a Research and Development Engineer in practice for almost ten years. He is currently an Associate Professor of electrical engineering with the Department of Electronics, Faculty of Electrical Engineering and Computer Science, VSB-Technical University of Ostrava. His research interests include DSC-based control systems, sensorless and sensor fault tolerant control of AC drives, applications of observers, estimators, and soft computing methods in the control of electrical drives.

PAVEL BRANDSTETTER was born in Ostrava, Czech Republic, in June 1955. He received the M.Sc. and Ph.D. degrees in electrical engineering from the Brno University of Technology, Czech Republic, in 1979 and 1987, respectively. He is currently a Full Professor of electrical machines, apparatus and drives and the Dean of the Faculty of Electrical Engineering and Computer Science, VSB-Technical University of Ostrava. His research interests include modern control methods of ac drives, for example, sensorless control of the IM and PMSM drives using different types of the observers.

BACH HOANG DINH received the B.E. and M.E. degrees in electrical engineering from Vietnam National University—Hochiminh City, in 1995 and 1998, respectively, and the Ph.D. degree in electrical engineering from Heriot-Watt University, Edinburgh, U.K., in 2009. He is currently the Head of the Electrical Engineering Department, Faculty of Electrical-Electronic Engineering, Ton Duc Thang University. His research interests include intelligent and optimal control, computer vision, robotics, power electronics, SCADA, and industrial communication networks. He is a member of the IEEE Industrial Electronics Society.